ARTICLE

Received 00th January 20xx, Accepted 00th January 20xx

DOI: 10.1039/x0xx00000x

Ultralow Thermal Conductivity through the interplay of composition and disorder between thick and thin layers of Makovickyite structure

Srikanth Balijapelly,^a Ashlee Hauble,^b Mathew Pollard,^c Morgane Poupon,^d Váčlav Petříček,^d Jeremy Lee Watts,^e Yew San Hor,^c Susan M. Kauzlarich,^b and Amitava Choudhury^{a, *}

Abstract Here we report the synthesis and characterization of three quaternary complex chalcogenides, $Ag_{0.68}Bi_{5.60}Cu_{1.06}S_9$ (I), $Ag_{0.62}Bi_{5.38}Cu_{1.56}S_9$ (II), and $Ag_{0.52}Bi_{4.48}Cu_2PbS_9$ (III). All the compounds in this homologous series crystallize in the C2/m space group and can be described as Pavonite structures. This structure type consists of alternating NaCl-like layers with varied thickness (P), separated by a pair of square pyramids. All the compounds reported here are synthetic analogues of the n=4 pavonite family and are known as makovickyite minerals. Compounds I – III possess complex crystal structures, consisting of mixed occupancies of Bi/Ag/Pb sites, as well as partially occupied Cu sites. These intrinsic assets lead to ultralow lattice thermal conductivities, in the range of $0.75 - 0.42 \text{ Wm}^{-1}\text{K}$ from 300 - 500 K, and make these materials promising candidates for thermoelectric applications. All three structures exhibit very narrow indirect band gaps of less than 0.5 eV as confirmed by DRS measurements. Charge transport properties are consistent with n-type semiconducting behavior with moderate electrical conductivities and large Seebeck coefficients. Low temperature electrical resistivity and Seebeck coefficient measurements are also performed on II. A promising figure of merit, zT, of 0.09 for I and II, 0.11 for III can be achieved at 4.75 K.

Introduction

Complex crystal structure and intrinsic structural disorder in ternary and quaternary chalcogenides have been demonstrated to have strong influences on thermoelectric properties, especially on lattice thermal conductivity. Minimization of total thermal conductivity is one of the key factors in developing high-performance thermoelectric materials, since the efficiency of thermoelectric materials is defined by the figure of merit, $zT = \frac{S^2 \, \sigma T}{\kappa_{total}}, \quad \text{where S is Seebeck coefficient, } \sigma \text{ is electrical conductivity, } \kappa_{total} \text{ is total thermal conductivity and } T \text{ is the absolute temperature. All these properties are interrelated via carrier concentration, making it difficult to isolate and improve one without negatively impacting another. For example, higher electrical conductivity is associated with lowering of the Seebeck coefficient and increasing the electronic component of$

the thermal conductivity. 1,3-5 Given the correlated nature of these properties, one strategy to increase zT is to focus on lattice thermal conductivity, which does not depend on carrier concentration. Synthesizing new compounds is in the hands of solid state chemists where lattice thermal conductivity can be minimized without adversely affecting S or σ . Strategies to reduce lattice thermal conductivity often rely on approaches that scatter phonons without affecting electrical conductivity and include defect engineering, such as point defect creation, grain boundaries, nano structuring, disorder and structural complexity. Additionally, compounds with lattice anharmonicity originating from stereo-active lone pairs located on heavy elements such as Bi, Sb, and Pb make ideal candidates to achieve ultra-low thermal conductivity. 6,7 All of these strategies to minimize thermal conductivity can be implemented in complex chalcogenides, which highlights the fact that identifying an appropriate family of crystal structures is crucial to discovering a high efficiency thermoelectric material.

Among several complex chalcogenide structures, the pavonite mineral family exhibits a high degree of structural and compositional diversity. The Pavonite family of compounds possesses three-dimensional (3-D) structure with layer-like modules stacked through bridging S atoms. The thin slab, called the 'a' layer, consists of paired square pyramids of ${\rm BiS}_5$ and the thick slab, called an incremental slab, is comprised of ${\rm BiS}_6$ octahedra which can have varied number of octahedra 'n' (in 'P' series) along the diagonal direction. The idealized unsubstituted homologues of the pavonite family can be described by the

Electronic Supplementary Information (ESI) available: The cif files of the compounds I-III. Tables of refinement parameters and atomic coordinates, equivalent isotropic and anisotropic displacement parameters for I-III. Figures of PXRD, TG-DSC, Hall plot, reciprocal lattice, and PDF plots. See DOI: 10.1039/x0xx00000x

 $^{^{}o}$ Department of Chemistry, Missouri University of Science and Technology, Rolla, MO 65409, USA

^bDepartment of Chemistry, One Shields Avenue, University of California, Davis, California 95616, United States

^cDepartment of Physics, Missouri University of Science and Technology, Rolla, MO 65409, USA

 $[^]d$ Institute of Physics, Czech Academy of Sciences, Na Slovance 2, 182 21 Prague, Czech Republic

^eDepartment of Materials Science and Engineering, Missouri University of Science and Technology, Rolla, MO 65409, USA

general formula $Ag^{ab}_{n-1}Bi^{a}_{4}Bi^{ab}Bi^{b}_{n+2}S_{2n+10}$ (for Z=1, formula unit), where $n=2-11.^{9}$ Because of their high tolerance of specific crystallographic sites for cations of different radii, a wide range of compositions can be derived and synthesized by incorporating transition as well as main group metals, Cu, Mn, Pb, In, Sb and Sn and so on. $^{11-24}$

Recently, several pavonite compounds were investigated and displayed promising thermoelectric properties. 11-16,19,25 For example, the Kanatzidis group has investigated $AgBi_3S_5$ which belongs to the ⁵P pavonite family and features remarkably low lattice thermal conductivity (0.6 Wm⁻¹K⁻¹) at room temperature due to double rattling phonon modes of Bi and Ag atoms. 17 $CdMBi_4Se_8$ (M = Pb/Sn) belongs to the n = 3 pavonite family with ultralow thermal conductivity of 0.58 Wm⁻¹K⁻¹ at 320 K and a peak zT of 0.63 for CdPbBi₄Se₈ at 850 K.¹⁸ Pavonites containing alkali ions (5P) $ASn_2Bi_5S_{10}$ (A = Li/Na) show low thermal conductivities in the range of 0.6 – 0.8 Wm⁻¹K⁻¹. ¹⁵ Intrinsic high frequency thermal vibration of interstitial Cu atoms in the lattice were proven to scatter phonons effectively in the $Cu_{x+y}Bi_{5-y}Q_8$ (Q = S, Se) series.^{26,27, 28} All these attributes make pavonite compounds an interesting class of materials for further investigation. However, several compositions have yet to be studied and the origin of the low thermal conductivity understood.

In this work, we have identified a ⁴P pavonite series also known as makovickyite family which has an idealized formula of $Ag_{1.5}Bi_{5.5}S_9$ (Z = 2, formula), in which Ag occupies an octahedral site in the thin layer as well as substituting on the Bi site in the thick layer.⁹ However, when Ag is replaced by Cu⁺, the Cu⁺ can occupy both tetrahedral and interstitial sites in the thin layer (a), along with heterotopic substitution in the thick layer. 29,30 When both Cu and Ag are present in the structure, Ag may or may not be present in the thin layer^{8,9,31-33} and if the amount of Cu is more (1.5 to 2 per formula unit, Z = 2), Cu atoms can substitute with statistical disorder and partial occupancy on crystallographic sites in the thin layer.³³ Substitution of excess Pb and Cu for Bi adds additional complexity, as one of the cell axes doubles resulting in a Cu-ordered structure similar to cupromakovickyite minerals.31,32 Taking cue from these observations we sought to synthesize analogues of makovickyite/cupromakovickyites with varying amounts of Cu while keeping the content of Ag relatively constant to study the effect of disorder in the lattice on thermal conductivity. We also substitute Pb in one of the compositions to evaluate the effect of lattice anharmonicity on the lattice thermal conductivity. Thus, in this manuscript we are reporting the synthesis, structural characterization, and thermoelectric properties of compositions $Ag_{0.68}Bi_{5.60}Cu_{1.06}S_9$ (I), $Ag_{0.62}Bi_{5.38}Cu_{1.56}S_9$ (II), $Ag_{0.52}Bi_{4.48}Cu_2PbS_9$ (III) with Ag/Cu ratio of 1.56 (I), 2.51(II), and 3.84(III), respectively. Measurements of physical properties exhibited ultra-low thermal conductivities (<0.8 Wm⁻¹K), high Seebeck coefficient values, and moderate electrical conductivities, which give rise to reasonably good thermoelectric figures of merit for compounds, I - III, at moderately low temperatures.

Experimental

Synthesis

Compounds, I – III, were synthesized by melting stoichiometric combinations of high purity Cu (Aldrich 99%), Ag (Alfa Aesar 99.9%), Bi (Cominco electronic materials), Pb (Alfa Aesar 99.9%), and S (Alfa Aesar 99.99%) powders. All the powder precursors were weighed accordingly and loaded into 12 mm diameter quartz ampoule (total weight of 3 g) and flame sealed under vacuum. The sealed ampoules were heated to 700 °C at a rate of 20 °C/h and dwelled for four days before cooling to room temperature at a rate of 35 °C/h. A silvery single ingot was obtained in all cases. Appropriate crystals were picked from crushed large ingots and used for single-crystal X-ray diffraction. Well-ground powder samples were used for further characterizations.

Single crystal X-ray diffraction

High quality single-crystals from I, II, and III were mounted on a Bruker smart apex diffractometer equipped with a sealed tube X-ray source with Mo–K α radiation (λ = 0.71073 Å) using a glass fiber. Room temperature diffraction data were collected using SMART³⁴ software with a step of 0.3° in ω scan and 20 s/frame exposure time. Data integration and absorption correction were achieved by using programs SAINT35 and SADABS35, respectively. SHELXS-97 and difference Fourier syntheses were used to solve the structures.36 Full-matrix least-squares refinement against $|F^2|$ was carried out using the SHELXTL-PLUS suite of programs.³⁵ For all compounds final refinements were carried out by SHELX-2018 incorporated in SHELXLe.37 Compounds I – III are the synthetic analogues of naturally occurring minerals.31-33 Our crystal structure solutions match very well with the reported ones for I and II. However, for III we did not get the doubled c-axis cell as the mineral structure,32 which could be due to the high temperature synthesis procedure adopted in the laboratory compared to natural crystal growth or due to slight deviation in our composition compared to the reported mineral. This was clear when all the reflections were projected on the reciprocal lattice, except for few spurious reflections all reflections fit into the normal cell. There were no systematic unaccounted reflections that would suggest a doubling of cell (Figure S1). All the compounds crystallize in C2/m space group (No.12). There are five wellbehaved S sites, out of which four are located on 4i and one on 2c and Bi can be located on three 4i site either fully or jointly occupied with Ag/Pb. Out of three Bi sites, Bi1 and Bi2 are located in the thick layer and Bi3 is located in the thin layer. In compound I, two 4i sites are fully occupied by Bi and the other by Bi/Ag (Bi1 and Ag1) jointly occupied with 80:20 ratio. Besides mixed occupancy with Bi, Ag is present in an octahedral 2a site (Ag2) in thin layer with 28% site occupancy. Additionally, there are two partially occupied Cu sites with 37% (Cu1, 4g) and 16% (Cu2, 4i) occupancy in the thin layer yielding a final charge balanced formula of Cu_{1.062}Ag_{0.68}Bi_{5.6}S₉ (I). For the refinement of II, three 4i sites have been assigned to Bi, among which one 4i site in the thick layer contains Ag with 31% site occupancy. Further refinements resulted in partial occupancy for Cu in four crystallographically unique positions in the thin layer, yielding a

Table 1: Crystal data and refinement details for I, II and III

	1	II	III
Empirical formula	$Ag_{0.68}Bi_{5.60}Cu_{1.06}S_{9}$	$Ag_{0.62}Bi_{5.38}Cu_{1.56}S_{9}$	$Ag_{0.52}Bi_{4.48}Cu_2PbS_9$
Formula weight	1599.53	1578.85	1615.13
Temperature	295(2) K	295(2) K	295(2) K
Wavelength	0.71073 Å	0.71073 Å	0.71073 Å
Crystal system	Monoclinic	Monoclinic	Monoclinic
Space group	C 2/m	C 2/m	C 2/m
Unit cell dimensions	a = 13.1938(15) Å	a = 13.227(2) Å	a = 13.356(2) Å
	b = 4.0566(5) Å	b = 4.0511(6) Å	b = 4.0339(6) Å
	c = 14.6417(17) Å	c = 14.637(2) Å	c = 14.841(2) Å
	b= 99.5290(10)°	b= 99.496(3)°	b= 99.915(2)°
Volume	772.84(16) ų	773.6(2) ų	787.6(2) Å ³
Z	2	2	2
Density (calculated)	6.874 g/cm³	6.778 g/cm ³	6.810 g/cm ³
Absorption coefficient	66.973 mm ⁻¹	65.014 mm ⁻¹	64.942 mm ⁻¹
Goodness-of-fit on F2	1.064	1.08	1.125
$R[I > 2\sigma(I)]^a$	R1 = 0.0294	R1 = 0.0323	R1 = 0.0415
wR (F2) (all data)b	wR2 = 0.0710	wR2 = 0.0740	wR2 = 0.0944

 $^{{}^{}a}R_{1} = \sum ||F_{0}| - |F_{c}|/\sum |F_{0}|.$

 $Table \ 2: Selected \ bond \ lengths \ (\mathring{A}) \ for \ (Ag_{0.68}Bi_{5.60}Cu_{1.06}S_9 \ \ \textbf{(I)}, \ Ag_{0.62}Bi_{5.38}Cu_{1.56}S_9 \ \ \textbf{(II)}, \ Ag_{0.52}Bi_{4.48}Cu_2PbS_9 \ \ and \ \textbf{(III)}$

I		II		III	
Moiety	Distances (Å)	Moiety	Distances (Å)	Moiety	Distances (Å)
Bi1 – S2	2.652(4)	Bi1 – S2	2.656(4)	Bi1 – S2	2.675(5)
Bi1 - S4#1	2.804(2)	Bi1 - S4#1	2.807(3)	Bi1 - S4 ^{#1}	2.810(3)
Bi1 - S1#3	2.8862(4)	Bi1 - S1#3	2.8911(5)	Bi1 - S1#3	2.8993(6)
Bi1 - S4	3.001(4)	Bi1 - S4	2.984(4)	Bi1 - S4	3.075(6)
Bi2 – S5	2.657(3)	Bi2 – S5	2.663(4)	Bi2 – S5	2.662(5)
Bi2 - S2#8	2.762(2)	Bi2 - S2#5	2.761(2)	Bi2 - S2 ^{#9}	2.765(3)
Bi2 - S4 ^{#2}	2.929(2)	Bi2 - S4 ^{#2}	2.927(3)	Bi2 - S4 ^{#2}	2.929(3)
Bi2 - S1	3.0133(6)	Bi2 - S1	2.9942(7)	Bi2 - S1	3.0290(9)
Bi3 - S3 ^{#13}	2.591(3)	Bi3 - S3 ^{#7}	2.596(3)	Bi3 - S3 ^{#11}	2.545(6)
Bi3 - S5#4	2.841(2)	Bi3 - S5#3	2.840(3)	Bi3 - S3 ^{#3}	2.779(5)
Bi3 - S3#3	2.857(2)	Bi3 - S3#3	2.855(2)	Bi3 - S5#4	2.983(5)
Ag2 – S5	2.232(3)			Pb1 - S3 ^{#11}	2.763(7)
Ag2 – S3 ^{#8}	2.902(2)			Pb1 - S5 ^{#3}	2.802(5)
				Pb1 - S3 ^{#3}	3.048(5)

Symmetry transformations used to generate equivalent atoms:

I #1 -x+1/2,-y-1/2,-z+1 #2 -x+1/2,-y+1/2,-z+1 #3 x+1/2,y+1/2,z #5 x-1/2,y-1/2,z #7 -x+1,-y,-z II #1 -x+1/2,-y-1/2,-z+1 #2 -x+1/2,-y+1/2,z #4 x+1/2,y-1/2,z #5 x,y+1,z #9 x-1/2,y+1/2,z #11 - x+1,-y,-z III #1 -x+1/2,-y-1/2,z #3 x+1/2,y+1/2,z #4 x+1/2,y-1/2,z #4 x+1/2,y-1/2,z #8 x-1/2,y-1/2,z #13 -x+1,-y,-z

 $^{{}^{}b}wR_{2} = \{\sum [w(F_{0}{}^{2} - F_{c}{}^{2})^{2}]/\sum [w(F_{0}{}^{2})^{2}]\}^{1/2}, w = 1/[\sigma^{2}(F_{0})^{2} + (\alpha P)^{2} + bP], \text{ where } P = [F_{0}{}^{2} + 2F_{c}{}^{2}]/3$

low R factor of 3.2% with a final charge balanced formula of $Cu_{1.56}Ag_{0.62}Bi_{5.38}S_9$ (II). A similar situation was observed in compound III, with one 4i site fully occupied by Bi and other two mixed occupied by Bi/Ag and Bi/Pb, respectively. Due to the similar X-ray scattering power of Bi (Z = 83) and Pb (Z = 82), free refinement of their occupancies was not reasonable, therefore, relative proportions according to stoichiometry used for the reaction were considered for further refinements. However, the position of Bi and Pb found to be split between Pb1 and Bi3 positions. By freely refining the Bi/Ag, R factor reduced significantly resulting 74% occupancy for Bi1 and 26% occupancy for Ag1 in 4i site in thick layer. Cu was found to partially occupy three different crystallographic sites yielding a final charge balanced formula Cu_{2.0}Ag_{0.52}PbBi_{4.48}S₉ (III). It is to be noted here that the use of split positions of Pb1 and Bi3 for III was evaluated against a model considering presence of anharmonic atomic displacement parameters (ADPs). The probability density function (P.D.F) of electrons was calculated from the refined anharmonic ADPs in the direct space to make sure that there were no termination effects in such maps. Such calculations indicated that the introduction of 4th order tensor leads to an unrealistic distribution of atoms in the Bi3/Pb1 site (Figure S2). On the other hand, the shape of the P.D.F with using only 3rd order term seemed to indicate split atom positions as we have used in our model (Figure S2). Moreover, it yielded a similar fit with the same number of refined parameters (Table S1). This means that we have a very reasonable support for split positions of Bi3/Pb1. The crystal data and refinement parameters are given in Table 1, and selected bond lengths are listed in Table 2. Atomic coordinates, isotropic and anisotropic displacement parameters are given in Tables S2-S7.

Powder X-ray diffraction

The room temperature powder X-ray diffraction was carried out on hand ground polycrystalline samples using PANalytical X'Pert

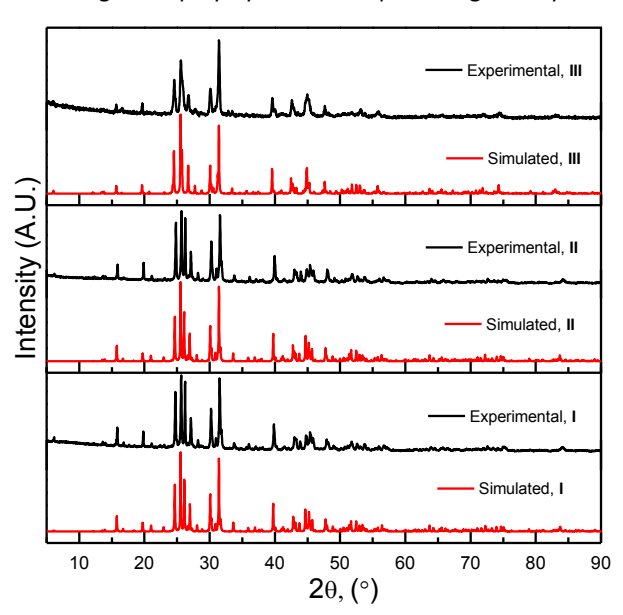


Figure 1. Comparison of experimental and simulated powder X-ray diffraction patterns for compounds $Ag_{0.68}Bi_{5.60}Cu_{1.06}S_9$ (I), $Ag_{0.62}Bi_{5.38}Cu_{1.56}S_9$ (II), and $Ag_{0.52}Bi_{4.48}Cu_2PbS_9$ (III).

diffractometer assembled with Cu K α anode and a linear array PIXcel detector over a 20 range of 5 to 90° with an average scanning rate of 0.0472° s⁻¹. Powder diffraction patterns of the well-ground as-synthesized samples are provided in Figure 1. Powder diffraction patterns were also collected on the hotpressed samples to see any phase transformations during the hot pressing (Figure S3).

Optical band gap measurements

Varian Cary 5000 UV-Vis-NIR spectrophotometer equipped with a praying mantis set up was used to measure the optical band gap using BaSO₄ powder (Fisher, 99.2%) as a reflectance standard. Diffuse reflectance spectroscopy was performed on compounds I-III in the wavelength range 200-2500 nm. Band gap values were estimated using a Tauc plot.³⁸ The equation $\alpha hv = A(hv - E_g)^m$ was employed to estimate the optical band gap, where α is absorption coefficient (Kubelka-Munk function),³⁹ hv is the photon energy, and m = 2 and ½ depending on whether the transition is direct or indirect. Compounds I-III exhibit linearity in hv vs $(\alpha hv)^{1/2}$ plot, suggesting that the samples possess indirect band gap. The band gap values are very narrow and below 0.5 eV as the curve was still riding in the

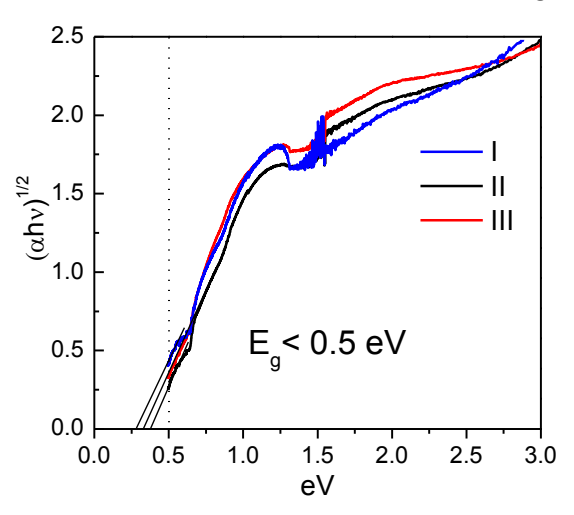


Figure 2: Diffuse reflectance spectra plotted as $hv vs (\alpha hv)^{1/2}$ for compounds $Ag_{0.68}Bi_{5.60}Cu_{1.06}S_9$, (I), $Ag_{0.62}Bi_{5.38}Cu_{1.56}S_9$ (II), $Ag_{0.52}Bi_{4.48}Cu_2PbS_9$ (III).

steep absorption edge at the lowest energy end of the measured wavelength (Figure 2).

Thermal analysis

TGA-DSC data were collected simultaneously from room temperature to $1050\,^{\circ}\text{C}$ with scan rate of $10\,^{\circ}\text{C}$ /min under a high purity argon atmosphere on approximately 20-30 mg of synthesized powder using a TA Instrument Q600SDT. DSC plots for compounds I, II and III are presented in Figure S1. All three compounds have similar melting points in the range $925-950\,^{\circ}$ K. Compound I displayed an endothermic peak at 540 K corresponding to a phase transition (Figure S4).

Sample preparation for physical property measurements

As-synthesized ingots were ground to fine powders using agate mortar in an argon filled glove box. The fine powders were loaded into a graphite die of 0.5 inch diameter. The die was placed in a hot press apparatus and the temperature was slowly

raised to 500 °C using a load of 35 MPa under high purity argon atmosphere for 20 minutes. The furnace was slowly cooled to 250 °C over a course of 2 hours and then the load was withdrawn. Hard cylindrical disks were obtained with more than 95% of the crystallographic density.

Seebeck and electrical resistivity measurements

Bars with dimensions ~10 mm x 2 mm x 1 mm were cut from the hot-pressed pellets using a Buehler diamond saw for high temperature resistivity and Seebeck coefficient measurements on a Linseis LSR-3. Measurements were done using a standard four-probe method under a helium atmosphere from 325 K to 475 K.

Low temperature electrical resistivity and Seebeck coefficients

diffusivity, C_P is specific heat, d is the density. Specific heat (C_P) is estimated by Dulong-Petit limit, $C_P = 3R/M$ (where R = ideal gas constant, M = average molar mass of each element) and density of all the samples were measured from the dimensions and masses. The calculated densities are $\sim 95\%$ of the theoretical densities.

Results and discussion

Structure description

Compounds, I – III, belong to the ⁴P pavonite homologous series and are also known as makovickyites. These structures have complex 3-D networks composed of two types of alternating

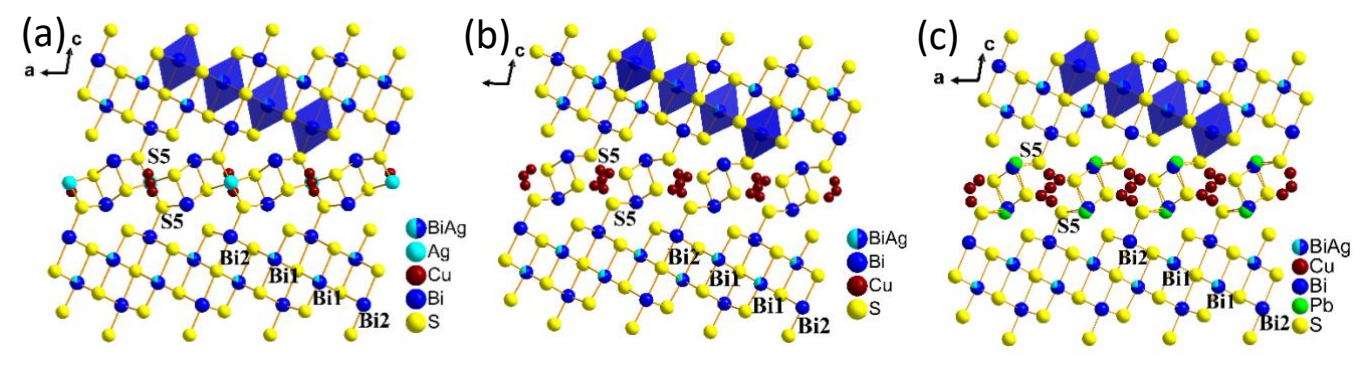


Figure 3. Makovickyite structures (⁴P pavonites) with four octahedra thick incremental layer (thick) and one octahedra thick non-incremental layer (thin) of compounds (a) Ag_{0.68}Bi_{5.60}Cu_{1.06}S₉, I; (b) Ag_{0.62}Bi_{5.38}Cu_{1.56}S₉, II; (c) Ag_{0.52}Bi_{4.48}Cu₂PbS₉, III.

were measured for compound II from 5 – 300 K. Bars of dimension 4 mm x 1.5 mm x 10 mm were measured in a Quantum Design PPMS thermal transport option (TTO) using a standard four probe method. Room temperature Hall measurements were performed on the same polished bar for compounds II and III using the PPMS system. Hall coefficients were derived from a hall resistance (ρ_{xy}) versus magnetic field (B) plot (Figure S5). Carrier concentration was determined from the Hall coefficient (R_H) using the formula $R_H = 1/ne$, where n is the carrier density and e is the charge.

Thermal conductivity measurements

Hot-pressed pellets were further polished and coated with graphite for thermal diffusivity $\alpha(T)$ measurements using the laser flash technique under high purity helium or argon atmosphere. Thermal diffusivity measurements were performed on compounds I - III from 300 to 475 K in Davis and from 475K to 800K for compounds II and III in Rolla. For compound I, our high temperature thermal diffusivity measurements failed as the pellet shattered after 540 K due to the presence of a phase transition at 540 K as evident from our DSC data (Figure S4). It is to be noted here that there is a slight mismatch of thermal conductivity data for compound III at 475 K (collected in two locations), presumably because of different pellets used from different batch of syntheses. Such differences may originate from small variations in stoichiometry and therefore carrier concentration due to human error during weighing of reactants for syntheses or slight differences in the density of hot-pressed pellets. Thermal conductivity was calculated using the formula $\kappa = \alpha(T).C_P.d$, where $\alpha(T)$ is thermal

slabs stacking perpendicular to the c-axis. The thick slab is composed of BiS₆ octahedra resembling a NaCl lattice and is four octahedra thick along the diagonal direction. The thin slab consists of pairs of BiS₅ square pyramidal pillars interconnected by either AgS₆ octahedra or interstitial copper atoms, depending on how much Cu is substituted for Ag (Figure 3). All the structures I, II, and III have three crystallographically unique Bi sites. Bi1 and Bi2 are present in slightly distorted octahedra within the thick layer, with the Bi1/2 - S bond lengths in the range 2.652(4) - 3.075(6) and 2.662(5) - 2.929(9) Å, respectively, and the Bi1 site is mixed occupied by Ag. Bi3 is part of the thin layer and is coordinated to five S atoms in a square pyramidal fashion, with four longer axial bonds in the range 2.855(2) - 2.983(5) Å and a shorter equatorial bond from 2.545(6) – 2.596(3) Å. In III, Bi3 site is split between Bi3 and Pb1. This finding is different from the naturally occurring mineral, wherein Pb takes up an independent position due to the doubling of the unit cell.³² All the Bi – S distances are in good agreement with several reported pavonite structures. 16,17 In I, because of the higher Ag content, some Ag is also present in the thin layer. In this case, Ag atoms adopt octahedral coordination and interconnect the Bi3S₅ square pyramidal pairs, with Ag2 − S bond distances ranging between 2.232(3) - 2.902(2) Å. Cu adopts linear and tetrahedral coordination in the makovickyite/cupromakovickyite structures. Accordingly, in compounds I and III, all the Cu atoms are tetrahedrally coordinated; however, in compound II, among four crystallographically distinct partially occupied Cu sites, Cu4 adopts linear coordination with a Cu4 - S distance of 2.251(4)

Å, while Cu1, Cu2 and Cu3 adopt flattened tetrahedral coordination in the thin layer, with the Cu - S bond lengths in the range 2.16(6)-2.61(5) Å. Local coordination environments for Bi and Cu for II are given in Figure 4. The thick and thin slabs are joined by a shared S5 atom resulting in a complex 3-D crystal structure. From the above discussion it is now amply clear that

Transport properties

We selected one of the compositions to measure low temperature electrical conductivity and Seebeck coefficients. Thus, low temperature electrical conductivity and Seebeck coefficient measurements were performed on compound II in the temperature range 5-300 K (Figure 5). An increase in the

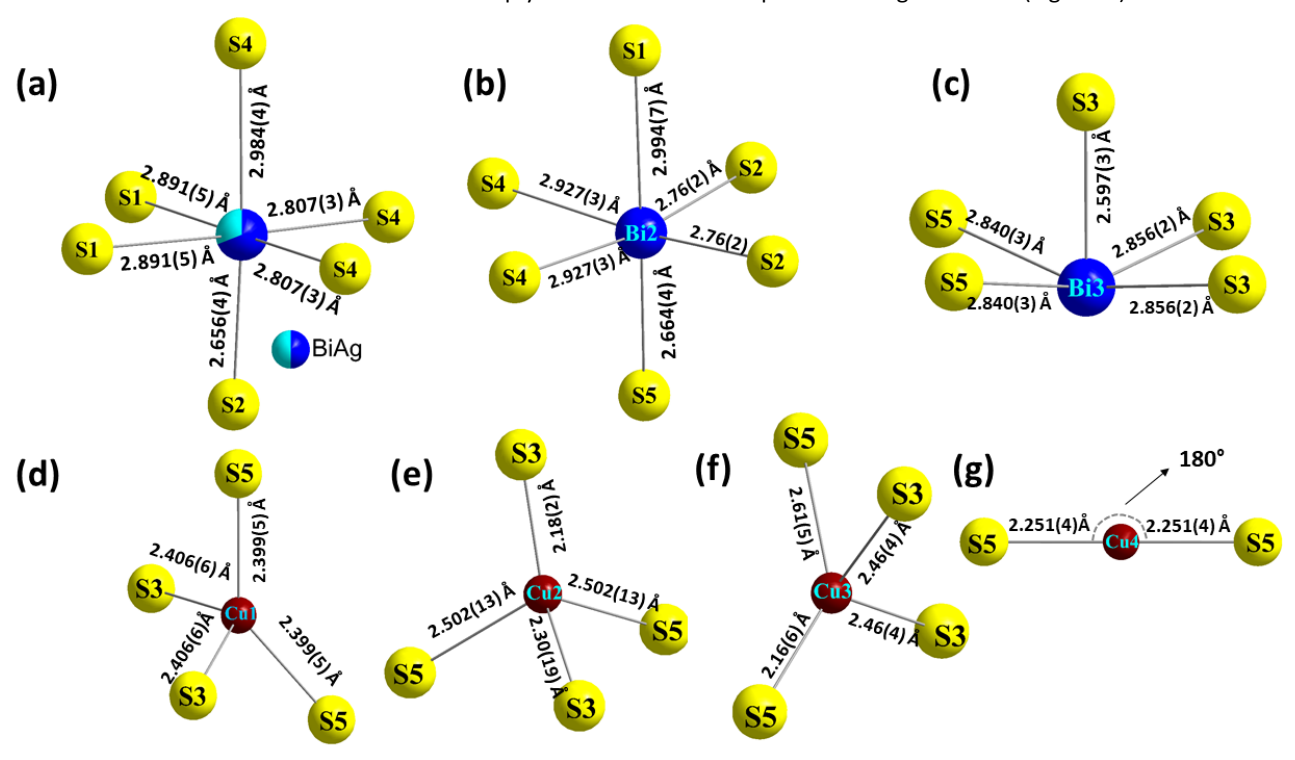


Figure 4: Coordination environments of Bi and Cu in Ag_{0.62}Bi_{5.38}Cu_{1.56}S₉ (II).

makovickyite structures offer excellent freedom in terms of tunable compositions and development of disorder as a function of Cu and Pb substitution, which enable independent tuning of the electrical and thermal properties and make them ideal candidates for thermoelectric applications.

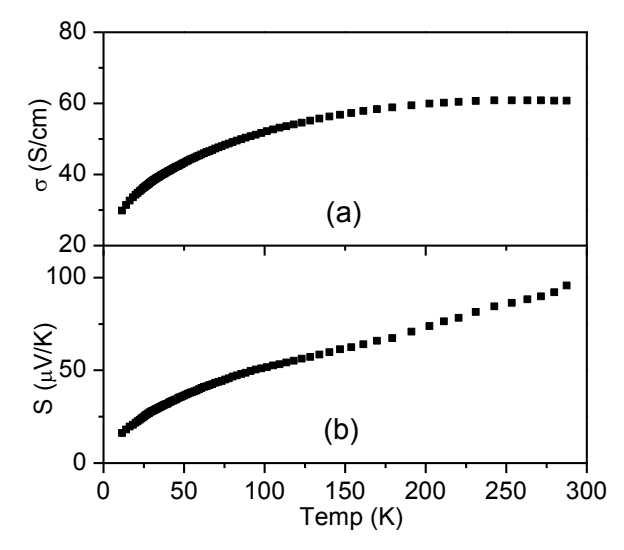


Figure 5. Low temperature charge transport measurements for compound $Ag_{0.62}Bi_{5.38}Cu_{1.56}S_9$, II (a) Electrical conductivity (b) Seebeck coefficient

electrical conductivity with temperature demonstrates the semiconducting nature of compound II. Compound II exhibits a moderate electrical conductivity of 60.7 S/cm at room temperature. Large negative Seebeck coefficients that increase linearly with temperature confirm the n-type charge carrier, reaching a value of 95 μ VK $^{-1}$ at 300 K. With these encouraging low-temperature transport properties we proceeded to investigate the high temperature TE properties of the three compositions.

Figure 6 shows the temperature dependence of thermoelectric properties for compounds I – III in the temperature range 300 – 500 K. Compounds I, II, and III exhibit room temperature electrical conductivities of 112, 95, and 65 S/cm, respectively, as shown in Figure 6a. Electrical conductivities did not change much in the measured temperature range and the values are comparable to many other pavonite compounds, for example 79 S/cm for CdPb₂Bi₄S₉ (n = 4)¹⁶ and 42 S/cm for AgBi₃S₅ (n = 5) at 300K.¹⁷

As observed in Figure 6b, the Seebeck coefficients for compounds I, II and III are negative and consistent with electrons being the dominant charge carriers. Seebeck coefficient of compound I is 70 μ V/K at 300 K and increased to 112 μ V/K at 500 K. The Seebeck coefficient of compound II is 81 μ V/K at 300 K and increased to 121 μ V/K at 500K whereas Seebeck coefficient of compound III is 100 μ V/K at 300K and

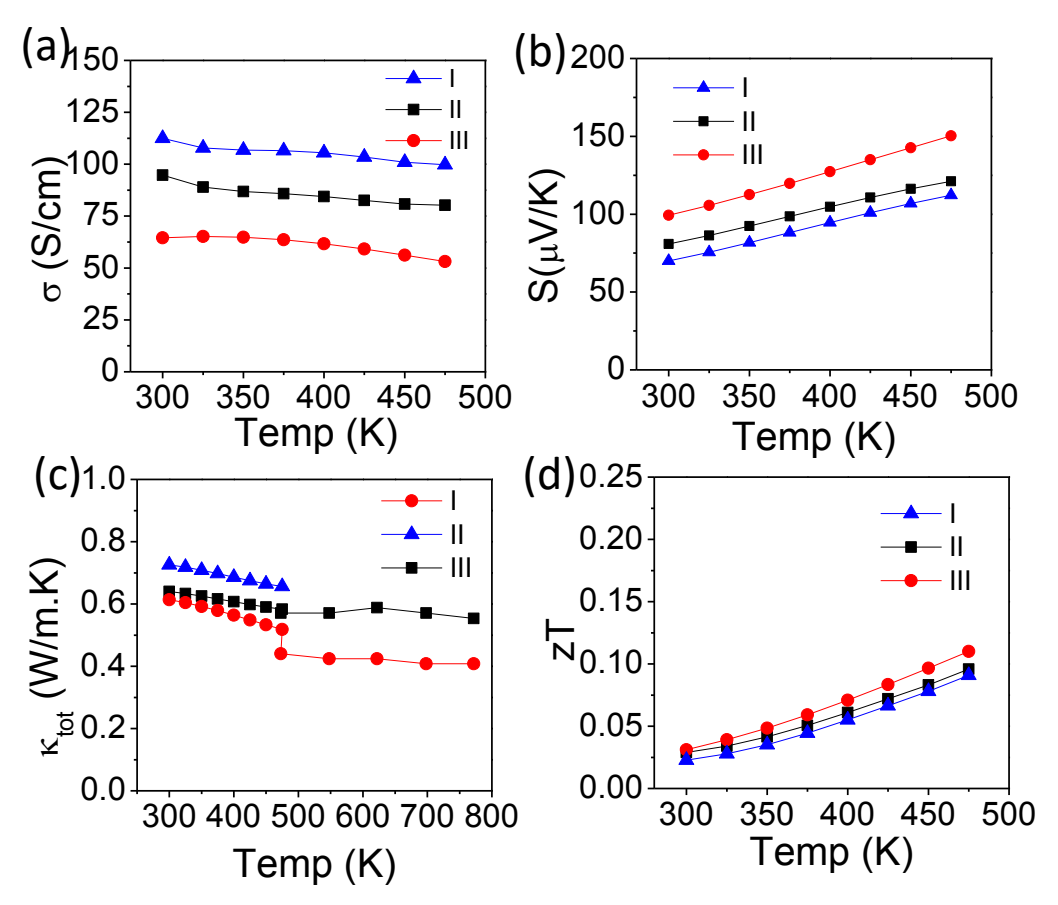


Figure 6: Temperature dependance of thermoelectric properties for compounds $Ag_{0.68}Bi_{5.60}Cu_{1.06}S_9$, I, $Ag_{0.62}Bi_{5.38}Cu_{1.56}S_9$, II, and $Ag_{0.52}Bi_{4.48}Cu_2PbS_9$, III; (a) Electrical conductivity, (b) Seebeck coefficient, (c) Thermal conductivity, (d) Figure of merit.

increased to 150 μ V/K at 500K. The power factor (*PF* = $S^2\sigma$) as a function of temperature for all the three compounds are given in Figure 7a. The power factors are in the range of 0.6 - 1.2 $\mu W.cm^{-1}K^2$ for compounds I – III which are in good agreement with other pavonites, such as $CdPb_2Bi_4S_9$ (n = 4).¹⁶ The trend observed in electrical conductivity and Seebeck coefficients can be correlated. The hall coefficient-derived carrier concentration values are of the order of 1.025×10²⁰ cm⁻³ for compound II and 1.55×10¹⁹ cm⁻³ for compound III. Slightly higher carrier concentration in compound II compared to compound III resulted in an increase in the electrical conductivity and decrease in the Seebeck coefficient, since the σ is directly proportional to the carrier concentration and S has an inverse relation with carrier concentration. Small variations in the values of electrical conductivity and Seebeck coefficient are observed in the room temperature data between the low temperature and above room temperature measurements because of the use of different batch of samples.

Figure 6c shows κ_{tot} in the temperature range 300 – 800 K for compound II and III and 300 – 500 K for compound I. These compounds possess ultra-low thermal conductivities in the range of 0.51 – 0.72 Wm $^{-1}$ K. The room temperature thermal conductivities are 0.72 Wm $^{-1}$ K for I, 0.64 Wm $^{-1}$ K for III. These values are comparable to the other reported pavonite family compounds, for example, 0.8 Wm $^{-1}$ K

in LiSn₂Bi₅S₁₀,¹⁵ 0.6 Wm⁻¹K in AgBi₃S₅,¹⁷ 0.78 Wm⁻¹K in CdPb₂Bi₄S₉¹⁶ and 0.67 – 1 Wm⁻¹K in MBi₄S₇ (M = Mn, Fe)¹⁹ and as well as to many state of the art chalcogenide thermoelectric materials, for example, κ_{tot} <1 Wm⁻¹K in Cu_{2-x}Se, 0.46 – 0.68 Wm⁻¹K in SnSe.^{40,41} The electronic contribution to the total thermal conductivity can be calculated using κ_{ele} = LoT (Wiedemann–Franz law). κ_{lat} can be calculated by subtracting the electronic contribution from the total thermal conductivity (κ_{tot} = κ_{ele} + κ_{lat}). The Lorenz number L is calculated using the Seebeck coefficient via the equation L= 1.5 + exp $\left[\frac{-|S|}{116}\right]$ where L

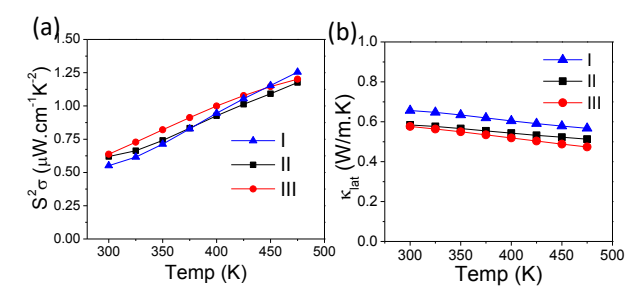


Figure 7. (a) Power factors (b) Lattice thermal conductivity (κ_{lat}) for Ag_{0.68}Bi_{5.60}Cu_{1.06}S9, I, Ag_{0.62}Bi_{5.38}Cu_{1.56}S9, II, and

is in 10⁻⁸ W Ω K⁻² and S is in μ V/K.⁴²

Lattice thermal conductivity, κ_{lat} , values for compounds, I-III, (Figure 7b) are close to the κ_{tot} values because of the negligible

electronic contribution, which corroborates well with the low electrical conductivities. The room temperature κ_{lat} values are 0.65 Wm $^{-1}$ K for I, 0.58 Wm $^{-1}$ K for II, and 0.57 Wm $^{-1}$ K for III. Though there are significant differences in the electrical conductivity and Seebeck coefficient values of compounds II and III, the κ_{lat} values are similar, which suggest that there may be opportunities to improve the electrical conductivity without negatively affecting the thermal conductivity.

The ultra-low and temperature independent thermal conductivity could originate from the very large anisotropic thermal vibration of partially occupied, disordered copper atoms, especially Cu1, Cu3 in compound II and Cu1, Cu2 in compound III. Additionally, for III, strong vibrational anharmonicity due to the presence of stereo-active lone pairs on Pb results in the lowest lattice thermal conductivity amongst the three compounds. These extremely low κ_{lat} values can be attributed to a combination of the complex electronic structure, mixed and partial occupancies, large unit cell volumes, and vibrational anharmonicities within the lattice. The partially occupied Cu atoms in the interstitial positions in the thin layer may be considered as rattling of atoms in a cage-like structure and acts as a source of enhance phonon scattering. 43,44 However, to confirm this hypothesis, the nature of Cu atoms in the interstitial positions needs to be evaluated using phonon dispersion calculations. The zT values calculated using the above transport properties are presented in Figure 6d. The zT values are 0.09 for I and II, 0.11 for III at 475K.

Conclusions

Three quaternary complex chalcogenides, Ag_{0.68}Bi_{5.60}Cu_{1.06}S₉ (I), $Ag_{0.62}Bi_{5.38}Cu_{1.56}S_9$ (II), $Ag_{0.52}Bi_{4.48}Cu_2PbS_9$ (III) were synthesized by substituting Cu and Pb for Bi in the makovickyite family with general formula $\mathrm{Ag}^{ab}{}_{n\text{-}1}\mathrm{Bi}^{a}{}_{4}\mathrm{Bi}^{ab}\mathrm{Bi}^{b}{}_{n\text{+}2}\mathrm{S}_{2n\text{+}10}.$ These materials are indirect-gap n-type semiconductors with band gaps < 0.5 eV. Inherent complex compositions and partial occupancies yield very low thermal conductivities < 0.75 W.m⁻¹K. Ultra-low thermal conductivity coupled with a large Seebeck coefficient and moderate electrical conductivity yielded a promising zT of ~ 0.1 at 475K. These pavonite phases would be ideal candidates for substitutions with various divalent and trivalent metal atoms for Bi to increase carrier concentration and electrical conductivity, while adding additional disorder to further retain the lattice thermal conductivity. The amount of interstitial Cu can also be adjusted to tune the thermoelectric properties accordingly. Furthermore, once the role Cu atoms play in phonon suppression is understood, one can design an appropriate system with balanced electrical and thermal properties to achieve a higher zT.

Acknowledgements

The authors, AC and SB, acknowledge the funding for this work from National Science Foundation (NSF) under grant number DMR- 1809128. AH and SMK acknowledge the support from NSF

(DMR-201156) for this work. AH also acknowledges NSF for her graduate fellowship.

Author Contributions

AC conceived the problem and supervised the work. SB synthesized, crystallographically characterized samples, made pellets for measurements and measured band gaps. AH and SMK helped with High temperature TE measurements, MP and YSH helped with low temperature TE measurements, JLW helped with hot-pressing and high temperature TC measurements. MP (Poupon) and VP helped with anharmonic refinements. SB wrote the manuscript and all the authors approved the manuscript and provided valuable inputs.

Conflicts of interest

There are no conflicts to declare.

Notes and references

- G. J. Snyder and E. S. Toberer, Nat. Mater., 2008, 7, 105– 114.
- X. L. Shi, J. Zou and Z. G. Chen, Chem. Rev., 2020, 120, 7399–7515.
- I.Terasaki, Compr. Semicond. Sci. Technol., 2011, 326– 358.
- 4 D. M. Rowe, CRC handbook of thermoelectric, 2018.
- 5 J. R. Sootsman, D. Y. Chung and M. G. Kanatzidis, *Angew. Chemie Int. Ed.*, 2009, **48**, 8616–8639.
- E. J. Skoug and D. T. Morelli, *Phys. Rev. Lett.*, 2011, **107**, 235901.
- 7 M. D. Nielsen, V. Ozolins and J. P. Heremans, *Energy Environ. Sci.*, 2013, **6**, 570–578.
- 8 W. G. Mumme, Neues Jahrb. Miner. Monatsh., 1990, 193–204.
- 9 W. Zak, L.; Fryda, L.; Mumme, W.G.; Paar, Neues Jahrb. fuer Mineral. Abhandlungen, 1994, **168**, 147–169.
- 10 J. M. Perez-Mato, L. Elcoro, E. Makovicky, D. Topa, V. Petříček and G. Madariaga, Mater. Res. Bull., 2013, 48, 2166–2174
- 11 Z. Z. Luo, C. S. Lin, W. D. Cheng, W. L. Zhang, Y. B. Li, Y. Yang, H. Zhang and Z. Z. He, *Cryst. Growth Des.*, 2013, 13, 4118–4124.
- 12 P. F. P. Poudeu and M. Ruck, *Acta Cryst. C*, 2005, **61**, i41-i43.
- 13 C. Anglin, N. Takas, J. Callejas and P. F. P. Poudeu, *J. Solid State Chem.*, 2010, **183**, 1529–1535.
- 14 S. Nakhal, D. Wiedemann, B. Stanje, O. Dolotko, M. Wilkening and M. Lerch, 2016, 238, 60–67.
- J. F. Khoury, S. Hao, C. C. Stoumpos, Z. Yao, C. D. Malliakas, U. Aydemir, T. J. Slade, G. J. Snyder, C. Wolverton and M. G. Kanatzidis, *Inorg. Chem.*, 2018, 57, 2260–2268.
- 16 J. Zhao, S. Hao, S. M. Islam, H. Chen, G. Tan, S. Ma, C. Wolverton and M. G. Kanatzidis, *Chem. Mater.*, 2019, 31, 3430–3439.
- 17 G. Tan, S. Hao, J. Zhao, C. Wolverton and M. G. Kanatzidis, *J. Am. Chem. Soc.*, 2017, **139**, 6467–6473.

- 18 J. Zhao, S. M. Islam, S. Hao, G. Tan, X. Su, H. Chen, W. Lin, R. Li, C. Wolverton and M. G. Kanatzidis, *Chem. Mater.*, 2017, 29, 8494–8503.
- 19 J. Labégorre, A. Virfeu, A. Bourhim, H. Willeman, T. Barbier, F. Appert, J. Juraszek, B. Malaman, A. Huguenot, R. Gautier, V. Nassif, P. Lemoine, C. Prestipino, E. Elkaim, L. Pautrot-d'Alençon, T. Le Mercier, A. Maignan, R. Al Rahal Al Orabi and E. Guilmeau, Adv. Funct. Mater., 2019. 29, 1904112.
- 20 M. Ruck and P. F. Poudeu, Zeitschrift fur Anorg. und Allg. Chemie, 2008, **634**, 475–481.
- 21 K. G. S. Ranmohotti, H. Djieutedjeu, J. Lopez, A. Page, N. Haldolaarachchige, H. Chi, P. Sahoo, C. Uher, D. Young and P. F. P. Poudeu, *J. Am. Chem. Soc.*, 2015, **137**, 691–698.
- 22 K. G. S. Ranmohotti, H. Djieutedjeu and P. F. P. Poudeu, J. Am. Chem. Soc., 2012, **134**, 14033–14042.
- 23 M. F. Wang, S. M. Jang, J. C. Huang and C. S. Lee, J. Solid State Chem., 2009, 182, 1450–1456.
- 24 W. G. Mumme and J. A. Watts, Acta Crystallogr. Sect. B Struct. Crystallogr. Cryst. Chem., 1980, 36, 1300–1304.
- 25 W. Choe, S. Lee, P. O'Connell and A. Covey, *Chem. Mater.*, 1997, 9, 2025–2030.
- 26 S. Qu, J. Zhao, Z. Jiang, D. Jiang and Y. Wang, *Mater. Chem. Front.*, 2021, 5, 1283–1294.
- 27 J. Y. Cho, H. Mun, B. Ryu, S. Il Kim, S. Hwang, J. W. Roh, D. J. Yang, W. H. Shin, S. M. Lee, S. M. Choi, D. J. Kang, S. W. Kim and K. H. Lee, *J. Mater. Chem. A*, 2013, 1, 9768–9774.
- 28 J. Y. Hwang, M. W. Oh, K. H. Lee and S. W. Kim, *J. Mater. Chem. C*, 2015, **3**, 11271–11285.
- 29 M. Ohmasa, M. Jahrb. Mineral. Monatsh., 1973, 227
- 30 K. Tomeoka, M. Ohmasa and R. Sadanaga, *Mineral. J.*, 1980, **10**, 57–70.
- 31 D. Topa and W. H. Paar, *Can. Mineral.*, 2008, **46**, 503–514
- 32 D. Topa, E. Makovicky and T. Balić-Žunić, *Can. Mineral.*, 2008, **46**, 515–523.
- 33 M. Nagashima, T. Armbruster, Y. Izumino and K. Nakashima, *Neues Jahrb. fur Mineral. Abhandlungen*, 2013, **191**, 75–81.
- 34 Bruker- SMART. Bruker AXS Inc., Madison, Wisconsin, USA. 2002.
- 35 Bruker-SAINT and SADABS, and SHELXTL. Bruker AXS Inc., Madison, Wisconsin, USA, 2008
- 36 G. M. Sheldrick, Acta Crystallogr. Sect. A Found. Crystallogr., 2008, 64, 112–122.
- 37 C. B. Hübschle, G. M. Sheldrick and B. Dittrich, J. Appl. Crystallogr., 2011, 44, 1281–1284.
- 38 J. Tauc, Mater. Res. Bull., 1968, 3, 37-46.
- 39 P. Kubelka and F. Z. Munk, *Tech. Phys.*, 1931, **12**, 593–
- 40 H. Liu, X. Shi, F. Xu, L. Zhang, W. Zhang, L. Chen, Q. Li, C. Uher, T. Day and G. Snyder Jeffrey, *Nat. Mater.*, 2012, 11. 422–425
- 41 L. D. Zhao, S. H. Lo, Y. Zhang, H. Sun, G. Tan, C. Uher, C. Wolverton, V. P. Dravid and M. G. Kanatzidis, *Nature*, 2014, **508**, 373–377.
- 42 H. S. Kim, Z. M. Gibbs, Y. Tang, H. Wang and G. J. Snyder, *APL Mater.*, 2015, **3**, 041506.
- 43 G. S. Nolas, D. T. Morelli and T. M. Tritt, Annu. Rev. Mater. Sci., 1999, 29, 89–116.

44 K. Suekuni, C. H. Lee, H. I. Tanaka, E. Nishibori, A. Nakamura, H. Kasai, H. Mori, H. Usui, M. Ochi, T. Hasegawa, M. Nakamura, S. Ohira-Kawamura, T. Kikuchi, K. Kaneko, H. Nishiate, K. Hashikuni, Y. Kosaka, K. Kuroki and T. Takabatake, Adv. Mater., 2018, 30, 10–15